

1 **Quantitative Proteomics of Enriched Esophageal and Gut Tissues from the Human**

2 **Blood Fluke *Schistosoma mansoni* Pinpoints Secreted Proteins for Vaccine Development**

3  
4 Leandro X. Neves <sup>1</sup>, R. Alan Wilson <sup>2</sup>, Philip Brownridge <sup>3</sup>, Victoria M. Harman <sup>3</sup>, Stephen  
5 W. Holman <sup>3</sup>, Robert J. Beynon <sup>3</sup>, Claire E. Eyers <sup>3</sup>, Ricardo DeMarco <sup>4</sup> and William Castro-  
6 Borges <sup>1\*</sup>

7  
8 <sup>1</sup> Departamento de Ciências Biológicas, Universidade Federal de Ouro Preto, Campus Morro  
9 do Cruzeiro, Ouro Preto, Minas Gerais, Brasil.

10 <sup>2</sup> Centre for Immunology and Infection, Department of Biology, University of York,  
11 Heslington, York, United Kingdom.

12 <sup>3</sup> Centre for Proteome Research, Department of Biochemistry, Institute of Integrative  
13 Biology, University of Liverpool, Liverpool, L69 7ZB, United Kingdom.

14 <sup>4</sup> Instituto de Física de São Carlos, Universidade de São Paulo, São Carlos, Brasil.

15  
16 \*Correspondence should be addressed to:

17 William de Castro Borges, Departamento de Ciências Biológicas, Instituto de Ciências  
18 Exatas e Biológicas, sala 58, Laboratório de Enzimologia e Proteômica. Universidade Federal  
19 de Ouro Preto, Campus Morro do Cruzeiro. Ouro Preto - Minas Gerais - Brasil. CEP: 35.400-  
20 000. Phone: +55 31 3559 1705

21 FAX: +55 31 3559 1680;

22 e-mail: wborges@ufop.edu.br

26 **ABSTRACT**

27 Schistosomes are blood-dwelling helminth parasites that cause schistosomiasis, a debilitating  
28 disease resulting in inflammation and, in extreme cases, multiple organ damage. Major  
29 challenges to control the transmission persist and the discovery of protective antigens remains  
30 of critical importance for vaccine development. Rhesus macaques can self-cure following  
31 schistosome infection, generating antibodies that target proteins from the tegument, gut and  
32 esophagus, the last of which is the least investigated. We developed a dissection technique  
33 that permitted increased sensitivity in a comparative proteomics profiling of schistosome  
34 esophagus and gut. Proteome analysis of the male schistosomes esophagus identified 13  
35 proteins encoded by microexon genes (MEG), eleven of which were uniquely located in the  
36 esophageal glands. Based on this and transcriptome information, a QconCAT was designed  
37 for absolute quantification of selected targets. MEGs 12, 4.2, 4.1 and Venom allergen-like  
38 protein 7 were the mostly abundant, spanning over 245-6 million copies per cell, while  
39 aspartyl protease, palmitoyl thioesterase and a galactosyl transferase were present at <1  
40 million copies. Antigenic variation by alternative splicing of MEG proteins was confirmed  
41 together with a specialised machinery for protein glycosylation/secretion in the esophagus.  
42 Moreover, some gastrodermal secretions were highly enriched in the gut, while others were  
43 more uniformly distributed throughout the parasite, potentially indicating lysosomal activity.  
44 Collectively, our findings provide a more rational, better-oriented selection of schistosome  
45 vaccine candidates in the context of a proven model of protective immunity.

46

47 **Keywords:**

48 *Schistosoma mansoni*; esophageal gland; gastrodermis; microexon genes; quantitative  
49 proteomics; QconCAT

50

51 **Introduction**

52 Schistosomes are blood-dwelling helminth parasites responsible for a chronic and debilitating  
53 disease in individuals living in tropical and subtropical regions <sup>1</sup>. At least 165 million people  
54 are estimated to be infected in Africa alone, largely based on detection of eggs in urine or  
55 faeces. However, the recent use of more sensitive diagnostics in areas of low transmission  
56 (<50% prevalence) indicates that cases of schistosomiasis may be underestimated by a factor  
57 of 1.5 to 6-fold when circulating cathodic antigen tests are compared to classical Kato-Katz  
58 technique <sup>2</sup>. A single drug, Praziquantel, is currently available to treat infected individuals but  
59 has limitations, notably its lack of activity against juvenile worms <sup>3</sup>. Chemotherapy invariably  
60 is started when the inflammatory responses against the eggs lodged in the host liver,  
61 intestines and bladder have already been established. In addition, data for 2016 suggest that  
62 annually the drug is only reaching ~36% of people needing treatment. In this situation, a  
63 protective vaccine to prevent infection remains of critical importance in the battle to combat  
64 schistosomiasis <sup>4</sup>.

65 The rhesus macaque (*Macaca mulatta*) is unusual among the various vertebrate hosts that  
66 schistosomes can infect, in that it can eliminate adult worms. A mature *Schistosoma mansoni*  
67 population establishes with oviposition peaking at week 9 before a gradual decline between  
68 12 and 18 weeks <sup>5</sup>. Recovery of surviving worms by perfusion of the hepatic portal system  
69 reveals that they have ceased feeding and are starving to death. Classical immunoproteomics  
70 (2D-PAGE and western blotting) indicated potential antibody targets in both surface  
71 tegument and secreted gut protein preparations <sup>5</sup>. A more detailed investigation of *S.*  
72 *japonicum* infection in the Rhesus macaque has further illuminated the possible mechanisms  
73 that prevent blood feeding. The esophageal lumen, surrounded by the anterior and posterior  
74 esophageal glands, was identified as the primary site for interaction with a potent humoral  
75 immune response <sup>6</sup>. Differential transcriptomics indicates that the gland secretions comprise a

76 cocktail of enzymes and a variety of proteins encoded by microexon genes (MEGs) <sup>7,8</sup>. We  
77 have documented that initial processing of ingested blood occurs in the esophageal lumen by  
78 mixing with the gland secretions <sup>9</sup>. Erythrocytes and platelets are lysed, while leucocytes are  
79 inactivated before they are propelled to the gut lumen where further digestion and absorption  
80 of nutrients take place <sup>10</sup>. Notably, the rhesus macaque seems able to block this initial blood  
81 processing by disrupting the release of gland secretions, ultimately leading the parasites to  
82 starvation <sup>6</sup>. To date, the function of these proteins has been inferred only from bioinformatic  
83 analyses of the encoding transcripts and their tissue pattern of expression <sup>6-8</sup>. An important  
84 step in the characterisation of proteins released into the esophageal lumen as potential  
85 immune targets is to determine their profile and relative abundance.

86 There are multiple challenges associated with the proteomic characterisation of esophageal  
87 gland secretions from schistosomes. Perhaps, the most important is that both anterior and  
88 posterior esophageal glands represent a tiny percentage of the whole worm body <sup>9</sup>.  
89 Consequently, constituents derived primarily from muscle tissues prevent identification of the  
90 unique set of gland products from whole worm extracts. Thus our recent investigation of the  
91 soluble protein composition of a *S. mansoni* preparation failed to detect any predicted gland  
92 constituents, attesting to their low abundance <sup>11</sup>. In addition, the prediction of multiple splice  
93 variants for MEG proteins <sup>12,13</sup> indicates the need for a more refined experimental design for  
94 sample preparation, combined with the utilization of modern, fast and sensitive mass  
95 spectrometric platforms for protein identification and quantification.

96 Here we tackle these challenges using a dissection technique to specifically target and enrich  
97 the esophageal gland for proteomic characterisation. Absolute quantification of selected  
98 protein targets, using QconCAT technology <sup>14,15</sup>, provided information on the abundance of  
99 gland constituents involved in blood processing. In addition, shotgun proteomics analysis  
100 confirmed that microexon genes expressed in the esophageal glands may be variably spliced.

101 Finally, a comparative analysis of the worm esophagus and posterior body (back end) served  
102 not only to highlight genuine gland products but also permitted the identification of proteins  
103 involved in nutrient acquisition in the lower alimentary tract. Overall, we believe our findings  
104 will provide the basis for a more rational and better-oriented selection of candidates of a  
105 vaccine against schistosome infection in the context of a proven model of protective  
106 immunity.

107

## 108 **Experimental section**

### 109 *Ethical Statement*

110 All procedures for maintenance of the *S. mansoni* life cycle and worm recovering were  
111 approved by the Ethics Committee on Animal Experimentation (Comissão de Ética no Uso  
112 de Animais – CEUA), Universidade Federal de Ouro Preto, protocol n°. 2011/55.

113

### 114 *Worm recovery and dissection*

115 Adult *S. mansoni* worms were obtained by portal perfusion of 45 day-infected mice using 10  
116 mM HEPES buffered RPMI-1640 medium, pH 7.4 (Sigma-Aldrich, USA), containing 4  
117 IU/ml of heparin. After extensive washes in pre-warmed medium (37 °C), parasites were  
118 instantly fixed in RNAlater<sup>®</sup> Solution (Invitrogen, UK) for protein stabilisation and stored at  
119 4 °C, as previously described<sup>7</sup>. Briefly, adult male worms immersed in ice-cold RNAlater<sup>®</sup>  
120 were carefully held and dissected using fine curved tweezers (Ideal Tek, Chiasso,  
121 Switzerland) and Vannas scissors (John Weiss, Milton Keynes, UK), under a  
122 stereomicroscope at x35 magnification. First, the oral sucker was removed by an incision at  
123 its posterior, at the very beginning of the esophagus. Next, a second cut along the line of the  
124 transverse gut released the esophageal fragment (ESO). The back end (BE) comprising the  
125 posterior third of the male body was excised for comparative analysis. Dissected fragments

126 were preserved in RNeasy<sup>®</sup> Solution at 4 °C until sample preparation, following the  
127 manufacturer's instruction. The detailed and illustrated dissection procedure is uploaded at  
128 protocols.io repository <sup>16</sup> (<https://www.protocols.io/>) and accessible via DOI  
129 dx.doi.org/10.17504/protocols.io.tq2emye. Biological replicates obtained from independent  
130 mouse infection, perfusion and worm dissection procedures provided material for individual  
131 shotgun and targeted proteomic analyses.

132

### 133 *Sample preparation and in-solution digestion*

134 ESO and BE fragments were washed twice in 1 mL of ice-cold PBS, pH 7.4, to remove  
135 RNeasy<sup>®</sup> Solution, as recommended by the manufacturer. Samples were sonicated in ice  
136 bath for 5 cycles of 10 second pulses at 30% amplitude (Sonics Vibra Cell<sup>™</sup>; Jencons  
137 Scientific Ltd, UK), with 50 seconds intervals. Total protein concentration was determined  
138 using a Coomassie Plus (Bradford) assay kit (Thermo Scientific, UK) by interpolation from a  
139 BSA standard curve, according to the manufacturer's instructions.

140 Sample aliquots equivalent to 20 µg of protein were processed through in-solution digestion  
141 protocol, essentially as described elsewhere <sup>17</sup>. Briefly, the aliquots were transferred to  
142 LoBind tubes (Eppendorf, USA) and made up to 100 µL by the addition of 25 mM  
143 ammonium bicarbonate (AMBIC). Protein denaturation was induced by the addition of 20 µL  
144 of RapiGest SF 1% w/v (Waters, UK) and heating at 80 °C for 10 min. Next, sample volume  
145 was adjusted to 180 µL with AMBIC before reduction (addition of 10 µL 60 mM  
146 dithiothreitol, 60 °C for 10 min) and alkylation (addition of 10 µL 180 mM iodoacetamide  
147 and incubation at room temperature for 30 min). MS-grade trypsin (Promega) was added at  
148 an enzyme:substrate ratio of 1:50 and digestion allowed to occur at 37 °C for 16 h.  
149 Trypsinolysis was terminated by addition of 1.5 µL trifluoroacetic acid. Acidified samples  
150 (pH<2) were then incubated at 37 °C for 45 min to precipitate RapiGest SF, which was later

151 removed by centrifugation at 13,000g for 15 min at 7 °C. Supernatant was recovered for LC-  
152 MS analysis.

153

#### 154 *nLC-ESI-MS/MS analysis of ESO vs BE region*

155 ESO and BE digests were analysed by a discovery-based proteomics approach using either a  
156 Q Exactive HF™ hybrid quadrupole-orbitrap (Thermo Scientific, Germany) or an Orbitrap  
157 Fusion™ Tribrid™ mass spectrometer (Thermo Scientific, Germany). Both instruments were  
158 coupled to Dionex™ UltiMate™ 3000 UHPLC system (Thermo Scientific, Germany) with  
159 the same column specifications. Briefly, 700 ng of digested samples were resolved over a 90-  
160 or 95-min gradient and analysed in positive mode using the Q Exactive HF and Orbitrap  
161 Fusion instruments, respectively. Spectral acquisition on the Q Exactive HF was performed  
162 using Top16 data-dependent acquisition (DDA) whereas Orbitrap Fusion operated in  
163 TopSpeed DDA mode with a 3-second cycle. In the latter platform, samples were analysed  
164 using CID and HCD activation capabilities of the instrument, and product ions were detected  
165 using the Ion Trap at rapid scan rate. Expanded LC-MS methods including a geLC-MS/MS  
166 analysis using a Q Exactive mass spectrometer (Thermo Scientific, Germany) for  
167 construction of a spectral library are available in the Supplementary Material S1.

168

#### 169 *Database search and label-free quantification*

170 *De novo* sequencing-assisted database searching<sup>18</sup> was performed using PEAKS Studio v8.5  
171 (Bioinformatics Solutions Inc, Canada). Firstly, spectral data were searched against *S.*  
172 *masoni* sequences deposited at GeneDB.org (downloaded at 17/10/2017) supplemented with  
173 protein sequences of esophageal hydrolases detected in a previous RNAseq experiment<sup>7</sup>  
174 (10,875 sequences; 5,942,443 residues). Esophageal MEG proteins were individually  
175 searched using a database composed of the sequences deposited in GeneDB and NCBI plus

176 putative alternative spliced variants generated *in silico* by combinatorial exon permutation  
177 (2,269 sequences; 223,997 residues). Precursors and product ion mass error tolerances were  
178 set respectively to 15 ppm and 0.02 Da, for the Q Exactive HF, or 10 ppm and 0.35 Da, for  
179 the Fusion instrument. Enzyme specificity was set to trypsin (P1 = K/R, except if P1' = P)  
180 allowing up to one missed cleavage site. Cysteine carbamidomethylation and dynamic  
181 methionine oxidation were set as peptide modifications. The quality threshold for Peptide-  
182 spectral match (PSM) was adjusted to keep the false discovery rate (FDR)  $\leq 0.01$ .

183 Relative label-free quantification for comparative ESO vs BE analysis was performed using  
184 Peaks Q enabling the exclusion of peptides with both modified and unmodified forms.  
185 Differentially abundant proteins with Benjamin–Hochberg adjusted *p*-values  $\leq 0.01$ , fold  
186 difference  $\geq 1.5$  and at least two unique peptides comprised the subset of ESO- or BE-  
187 enriched components.

188

#### 189 *Gene ontology and functional categorisation*

190 Differentially abundant proteins were subjected to gene ontology analysis using a PRO trial  
191 licenced Blast2GO v5 software <sup>19</sup>. Gene Ontology (GO) terms were mapped and the Fisher's  
192 Exact Test (FDR  $\leq 0.05$ ) assessed the enrichment of specific biological processes, molecular  
193 functions and cellular components amongst the proteins with higher relative abundances in  
194 the ESO compared to BE. Functional enrichment analysis on STRING v11 <sup>20</sup> provided  
195 KEGG pathways, keywords and GO terms over-represented in the list of differentially  
196 abundant proteins. Additional categorisation of cellular markers, namely the glycosyl  
197 transferases and gastrodermis secretion, was performed essentially as described elsewhere  
198 <sup>7,21</sup>.

199

#### 200 *QconCAT design, expression and purification*



201 Based on state of the art QconCAT technology <sup>14,15</sup> , an EsoCAT construct was designed by  
202 concatenating proteotypic peptides to obtain an artificial protein that served as the internal  
203 standard for simultaneous quantification of multiple analytes. The targets selected for  
204 absolute quantification comprised nine proteins with specific expression in the esophageal  
205 glands, previously validated by whole-mount *in situ* hybridization and confocal microscopy  
206 <sup>7,9</sup>, and detected by mass spectrometry.

207 Fifteen proteotypic peptides were selected from our in-house spectral library. Two additional  
208 peptide sequences were chosen based on their putative detectability, as predicted by the  
209 CONSeQuence algorithm <sup>22</sup>, and two N-terminal variant tryptic peptides were selected to  
210 investigate co-occurring MEG-12 isoforms (Supplementary Material S2). Uniqueness of  
211 proteotypic peptides was ascertained against the *Mus musculus* (UniProt UP000000589;  
212 60,177 sequences and 27,265,929 residues) and *Escherichia coli* BL21-DE3 (UniProt  
213 UP000002032; 4,156 sequences and 1,298,178 residues) proteomes, and GPM collection of  
214 common contaminants cRAP (116 sequences and 38,459 residues).

215 A minimum of two proteotypic peptides was selected for each target protein, with the  
216 exception of MEG-4.2 for which only one tryptic peptide had been identified during our  
217 spectral library construction. Moreover, sequences consisting of three amino acids found  
218 naturally flanking the proteotypic peptides in the endogenous target proteins were preserved  
219 in the EsoCAT construct to provide conditions for both analyte and internal standard to be  
220 evenly digested, as described elsewhere <sup>23</sup>. The complete EsoCAT primary structure  
221 comprised a N-terminal initiator methionine followed by the glufibrinopeptide B  
222 (EGVNDNEEGFFSAR), and a C-terminal hexahistidine tag (Supplementary Material S2).

223 For heterologous expression of EsoCAT, the synthetic gene was ligated into a pET21a  
224 plasmid vector (Eurofins Genomics, Germany) and transformed into BL21 ( $\lambda$ DE3) competent  
225 *E. coli* cells. EsoCAT expression was induced in the presence of 1 mM isopropyl  $\beta$ -D-1-

226 thiogalactopyranoside (IPTG) in minimal culture media containing  $^{13}\text{C}_6$  labelled lysine and  
227 arginine, as described elsewhere <sup>24</sup>. After 3.5 hours of induction, *E. coli* cells were collected  
228 by centrifugation (1,450 g, 15 min, 4 °C), resuspended in 50 mM AMBIC, pH 8.0, containing  
229 25 U/mL benzonase nuclease (Novagen), 1x Complete EDTA-free protease inhibitor tablet  
230 (Roche), and sonicated in an ice bath using 10 second pulses at 30% amplitude, with 50  
231 second intervals, until 130 joules was reached. After centrifuging the homogenate at 6,000 g,  
232 7 min, 7 °C, the EsoCAT protein present in the insoluble inclusion body pellets was  
233 solubilised in Buffer A (20 mM  $\text{NaPO}_4$ , 0.5 M NaCl, 10 mM imidazole, 6 M guanidine  
234 hydrochloride, pH 7.4) and filtered using a 1.2  $\mu\text{m}$  syringe filter.

235 EsoCAT purification was carried out using an AKTA start chromatography system (GE  
236 Healthcare) equipped with a 1 mL HisTrap™ HP column (GE Healthcare). System  
237 conditioning and washing were performed using Buffer A before bound proteins were eluted  
238 over a 20 min gradient of 0-100% Buffer B (20 mM  $\text{NaPO}_4$ , 0.5 M NaCl, 500 mM imidazole,  
239 6 M guanidine hydrochloride, pH 7.4), at a flow rate of 1  $\text{mL}\cdot\text{min}^{-1}$ . Eluted fractions  
240 containing EsoCAT were pooled and dialysed against 50 mM AMBIC containing 1 mM  
241 dithiothreitol. Purified EsoCAT preparation was supplemented with 0.1% (w/v) RapiGest SF  
242 (Waters) and aliquoted for storage at -20 °C in LoBind tubes (Eppendorf). Immediately  
243 before use, EsoCAT was thawed then heated to 60 °C in the presence of 3 mM dithiothreitol  
244 for protein reduction, thus preventing aggregate formation and precipitation.

245

#### 246 *In-solution co-digestion with EsoCAT internal standard*

247 Absolute quantification required the co-digestion of the proteome of interest and the  
248 QconCAT internal standard. Four replicates of a master mixture were prepared by spiking an  
249 estimated concentration of purified EsoCAT protein into 20  $\mu\text{g}$  of the ESO proteome. The  
250 master mixtures were subjected to our standard in-solution digestion protocol in the presence

251 of 100 fmol glufibrinopeptide B (Glufib B >98% purity; Severn Biotech) enabling the  
252 accurate quantification of the EsoCAT protein. In parallel, 20 µg digests containing only the  
253 ESO proteome were produced and used for serial dilution of the master mix by factors of  
254 1:10 and 1:100. This ensured the EsoCAT internal standard spanned a concentration range of  
255 two orders of magnitude (~0.15-150 fmol/µg of ESO proteome). LoBind tubes were used in  
256 all steps of this experiment.

257

#### 258 *Absolute quantification by SRM-MS*

259 Absolute quantification was performed on a nanoACQUITY UPLC™ system coupled to a  
260 Xevo TQS triple quadrupole mass spectrometer (Waters) set to Selected Reaction Monitoring  
261 (SRM) acquisition mode, with Q1 and Q3 operating at unit mass resolution. Up to one  
262 microgram of digested samples was loaded onto a Symmetry C<sub>18</sub> trap column (5 µm, 180 µm  
263 x 20 mm; Waters) and washed for 3 min, at a flow rate of 5 µL·min<sup>-1</sup>, with 0.1% (v/v) formic  
264 acid in water. Peptides were resolved on the analytical column HSS T3 nanoACQUITY C18  
265 (1.8 µm, 75 µm x 150 mm; Waters) over a 90 min linear gradient of 3-40% (v/v) MeCN in  
266 0.1% (v/v) formic acid, at a constant flow of 300 nL·min<sup>-1</sup>, at 35 °C. SRM acquisition was  
267 scheduled with 4 min windows and dwell times automatically adjusted to achieve ≥12  
268 sampling points per peak. Three to four product ions with highest relative intensity in  
269 experimental MS/MS spectra and  $m/z >$  precursor ion were selected to compose the list of  
270 transitions.

271

#### 272 *Data analysis of QconCAT assay*

273 Quantification of endogenous and surrogate peptides was performed using Skyline v4.2<sup>25</sup> by  
274 integrating extracted ion chromatograms for transitions monitored in light and heavy  
275 channels, respectively (Supplementary Material S2). An equivalent number of transitions

276 with random mass shifts (decoys) was also monitored allowing peak validation and FDR  
277 calculation by mProphet<sup>26</sup>. The concentration of labelled peptides was firstly assessed based  
278 on the reference Glufib B peptide. Analyte quantification was finally achieved using the light  
279 to heavy ratios observed in the isotopic dilution that fulfilled the following criteria: (i) closest  
280 1:1 ratio (never exceeding 10x fold) between the internal standard and endogenous analyte  
281 that exhibited a (ii) mProphet's FDR  $\leq 0.05$  score in at least three out of four replicates.  
282 To classify the performance of proteotypic peptides monitored by the SRM quantitative  
283 assay, we adopted the terminology described by Brownridge *et al* (2011)<sup>27</sup>. Accordingly,  
284 peptides were classified as Type 'A' when EsoCAT standard and endogenous analyte  
285 delivered high quality quantification data ('S<sup>+</sup>/A<sup>+</sup>' or 'standard positive, analyte positive'),  
286 Type 'B' when solely EsoCAT internal standard ('S<sup>+</sup>/A<sup>-</sup>') was observed, or Type 'C' when  
287 peptides could not be observed in either heavy or light channels ('S<sup>-</sup>/A<sup>-</sup>'). We refined this  
288 classification system by incorporating mProphet scores into the results. This divided Type  
289 'A' category into two further subgroups: Type 'A1' peptides successfully passed mProphet's  
290 5% FDR threshold and were used for protein quantification, whereas Type 'A2' peptides  
291 failed to give a clearer signal compared to decoy transitions (mProphet's FDR >0.05) and  
292 were removed.

293

## 294 **Results**

295 *Mass spectrometry analyses of ESO detect predicted esophageal gland proteins and sequence*  
296 *variation*

297 For the first time we were able to identify predicted esophageal gland proteins using a mass  
298 spectrometry-based approach on the ESO-enriched preparation. Detection of the group of  
299 MEG-encoded proteins, known to be specifically expressed in the gland cells<sup>7,28,29</sup>,  
300 confirmed the successful combination of shotgun proteomics and microdissection procedures.

301 Database search against deposited MEG-encoded sequences and alternative spliced variants  
302 generated by *in silico* exon permutation allowed the identification and study of MEG  
303 isoforms expressed in the esophageal gland. In parallel, database interrogation against *S.*  
304 *mansoni* protein sequences deposited in GeneDB resulted in a list of 4,024 proteins identified  
305 at  $\leq 1\%$  FDR. This was later reduced to 3,019 identities confidently assigned to at least two  
306 unique peptides.

307 Compositional analyses revealed that ESO and BE preparations share over 90% of the  
308 proteins confidently detected, whilst 141 and 54 proteins were exclusive to ESO and BE  
309 samples, respectively (Figure 1A). Among the proteins exclusively detected in the ESO  
310 sample, ten MEG proteins (MEG-3.4, MEG-4.1, MEG-4.2, MEG-5, MEG-8.1, MEG-8.2,  
311 MEG-8.4, MEG-14, MEG-15 and MEG-24) were confidently identified in this proteomic  
312 analysis, with  $\geq 2$  two PSM per protein at a false discovery rate  $\leq 1\%$ . Additionally, MEG-  
313 26.3, MEG-16 and MEG-12 were detected using less stringent filter criteria (1 PSM at  $\leq 1\%$   
314 FDR). Median peptide intensity values of unique peptides indicated that eleven of these MEG  
315 proteins are uniquely present in the worms' esophagus (Figure 1B; Supplementary Material  
316 S3). The remaining two namely MEG-5, a protein assigned to the tegument<sup>12</sup>, and MEG-24  
317 were detected at similar levels in the ESO and BE preparations normalised by their total  
318 protein content.

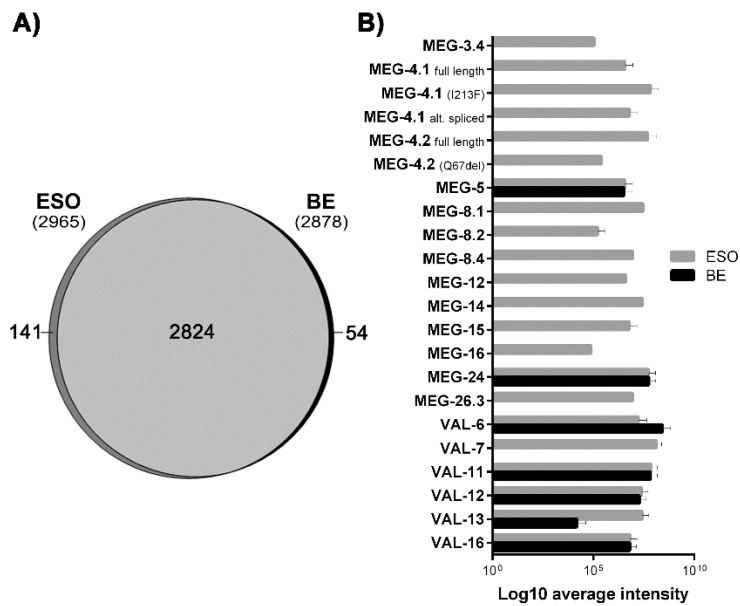


**Figure 1. Composite analyses of ESO and BE samples and differential abundance of esophageal signatures.** (A) Venn diagram indicating over 90% commonalities between the proteins confidently identified ( $\geq 2$  unique peptides;  $FDR \leq 0.01$  FDR) in the samples. A fraction of 141 proteins were detected only in the esophageal region (ESO) whilst 54 were present uniquely in the back end (BE) of adult male worms. (B) Abundance of unique peptides indicated that 11 out of 13 MEG are among the exclusively expressed in the schistosome esophagus, similarly VAL-7.

319

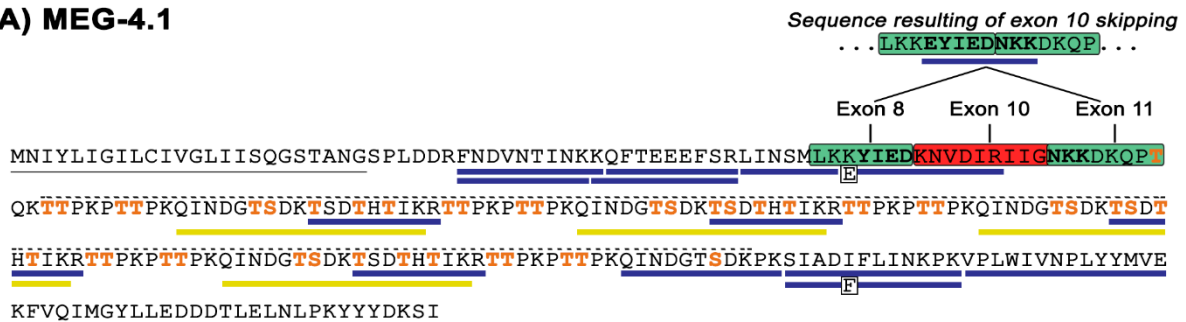
320 A second protein family investigated comprised the Venom Allergen-Like (VAL) proteins  
 321 since VAL-7 was the second gland-specific constituent discovered<sup>28</sup>. Our data confirmed  
 322 that VALs 7 and 13 were highly enriched in the ESO fraction compared to BE (Figure 1B),  
 323 whereas VALs 11, 12 and 16 had similar intensities in the two preparations, and VAL-6  
 324 found at higher levels in the BE.

325 Notably, our analysis produced not only the first MS-based detection of esophageal MEG  
 326 proteins but also delivered evidence of co-occurring isoforms of these gland secretions.  
 327 Sequence variations detected from the pool of worms includes alternative spliced sequences,  
 328 residue substitution and deletion. For instance, in comparison to the full-length of MEG-4.1  
 329 (GenBank accession AAA29855) we observed two amino acid substitutions, K57E and I213F  
 330 (Figure 2A), that matched other deposited transcript sequences (*e.g.* GenBank accession  
 331 AAP13803.1 and RefSeq XM\_018793269.1). Moreover, we gathered evidence for the co-  
 332 occurrence of MEG-4.1 isoforms resulting from alternative splicing. The peptide  
 333 ‘EYIEDKNVDIR’ present in the full-length sequence of MEG-4.1 is formed over an exon-  
 334 exon junction so that five N-terminal amino acids are encoded by exon 8, whereas the  
 335 following residues are encoded by exon 10 (27 bp). Hence, skipping exon 10 results in

336 ligation between exons 8/11 and omission of the 9-mer sequence ‘KNVDIRIIG’  
 337 (K62\_G70del), ultimately creating the new detectable tryptic product ‘EYIEDNKK’ (Figure  
 338 2A). It is noteworthy that exon 9 is rarely incorporated into MEG-4.1 transcripts and its  
 339 asymmetrical structure of 89 bp would produce an incomplete protein by disrupting the open  
 340 reading frame.

341 In a second case, the deletion of a glutamine residue (Q67) in MEG-4.2 (Smp\_085840.1) also  
 342 resulted in an alternative detectable proteotypic peptide for this esophageal protein. The  
 343 peptide ‘QLEEEQNPFHK’ is formed over the junction of exons 6/7 so that the second  
 344 glutamine of the sequence overlaps a splice site (Figure 2B). The alternative sequence,  
 345 ‘QLEENPFHK’, is obtained via an alternative splice site at the 3’-end of exon 6 that  
 346 changes the exon length from 21 to 18 bp, excluding the glutamine codon. Finally, peptide  
 347 identifications of MEG-14 matched alternative sequences shared by several known isoforms

### A) MEG-4.1



### B) MEG-4.2

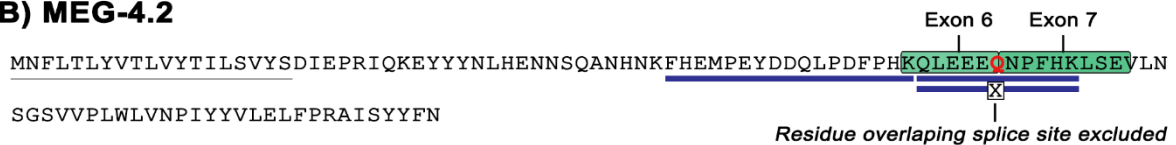


**Figure 2. Coverage of MEG-4.1 and 4.2 isoforms by shotgun proteomics.** (A) Full length sequence of MEG-4.1 (AAA29855) highlighting the mechanism of sequence variation of the detected isoforms. Amino acids encoded by exon 10 (red area) are deleted and direct ligation of exons 8 / 11 occurs (green area). Additionally, two residue substitutions (K57E and I213F) are indicated in the boxes. Residues in orange are predicted sites of O-glycosylation. Versions of MEG-4.1 incorporating exon 9 are rare and incomplete. The hashed line above the protein sequence indicates the tandemly repeated region. (B) MEG-4.2 protein sequence (Smp\_085840.1) with a residue encoded by an alternative splicing site (Q67) highlighted in red. The alternative sequence with Q67del is symbolised by the box with “X”. Peptide matches (FDR ≤0.01) are indicated by blue (≥2 PSM) and yellow (1 PSM) bars below the sequences.

348 produced by alternative splicing<sup>13</sup>. However, none of the five peptides detected are self-  
349 excluding, hence a unique isoform cannot be identified unambiguously. Instead, we observed  
350 that the peptide sequences are sometimes present in two, or in up to seven different MEG-14  
351 variants (Supplementary Material S3).

352

353 *QconCAT proteomics allows the abundance of gland secreted proteins to be determined*

354 We employed QconCAT-based quantification to capture the abundance of nine specific gland  
355 antigens in the ESO proteome. Seventeen out of 21 precursor ions monitored by SRM for  
356 absolute quantification were classified as Type 'A1' peptides (*i.e.* both analyte and surrogate  
357 peptides detected at mProphet FDR  $\leq 0.05$ ), thus being suitable for quantification  
358 (Supplementary Material S4). After removal of low scoring peptides (mProphet FDR  $>0.05$ ),  
359 MEG-4.1, MEG-8.2, MEG-15, VAL-7, aspartyl protease and palmitoyl thioesterase could be  
360 quantified by two of their proteotypic peptides and three other proteins (MEG-4.2, MEG-12  
361 and  $\beta$ -1,3-GalTase) by a single peptide standard each.

362 Using a mass-to-mass unit (ng/ $\mu$ g) the nine quantified proteins amounted to only  $\sim 0.5\%$  of  
363 the total protein found in the male worms' esophagus ( $0.5 \pm 0.17 \mu\text{g}$  per ESO fragment;  
364 Supplementary Material S4). However, since only 750 and 1,000 cells comprise the anterior  
365 and posterior glands<sup>9</sup> respectively, it is reasonable to expect that the gland products would  
366 not dominate an esophageal homogenate. Therefore, we estimated the number of protein  
367 copies per cell (cpc) as a better representation of our quantitative data since it normalised  
368 protein abundance to the number of producing cells (Figure 3).

369 When the data are viewed in this way, MEG-12, the only selected target demonstrated as  
370 expressed in the anterior gland, showed extraordinary abundance with over 245 million cpc,  
371 likely the integral of production and externalisation. VAL-7, MEG-4.2 and MEG-4.1 were  
372 also highly abundant with between 12.2-4.5 million cpc (Supplementary Material S4). The



373 remaining predicted secreted proteins, namely MEG-15, MEG-8,2, palmitoyl thioesterase and  
 374 aspartyl protease presented lower levels of 0.5-1 million cpc, whilst the endoplasmic protein  
 375  $\beta$ -1,3-GalTase showed the lowest cellular content of ~380 thousand cpc.

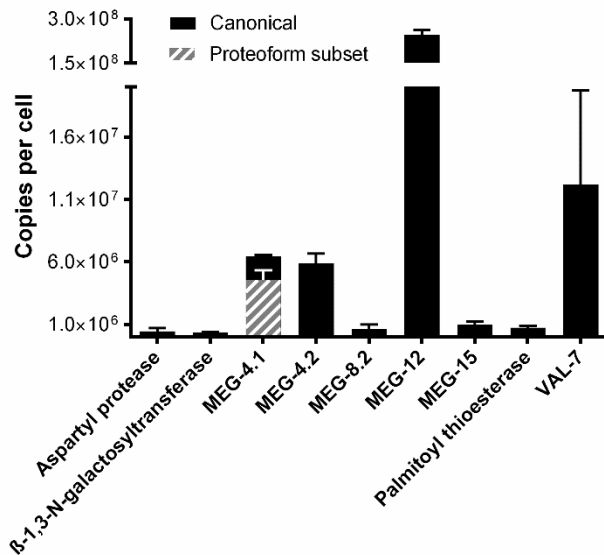


**Figure 3. Absolute quantification of esophageal gland proteins.** Protein copies normalised by the number of cells comprising the anterior and posterior esophageal glands in *S. mansoni* adult male worms, according to Li *et al* (2013). MEG-12, the only selected target demonstrated as being expressed in the anterior gland showed the highest abundance (~245 million cpc), followed by VAL-7 and MEGs-4.1 and 4.2. The EsoCAT construct allowed the quantification of MEG-4.1 via one peptide canonically expressed in the isoforms detected in this study and a second proteotypic peptide exclusive to an isoform subset (hashed bar).

376

377 Importantly, the knowledge about isoforms of MEG-4 family members must be considered in  
 378 the QconCAT analysis. The two proteotypic peptides of MEG-4.1 included in the EsoCAT  
 379 allowed the quantification of specific isoform subsets. Thus, MEG-4.1 variants containing an  
 380 isoleucine rather than a phenylalanine residue at position 213 accounted for 71% of all copies  
 381 detected using the second peptide, QINDGTSDKPK, conserved among known alternative  
 382 sequences (Figure 3; MEG-4.1 solid and hashed bar). In the case of MEG-4.2, we only  
 383 present the absolute quantification of the full length containing the QLEEEQNPFHK peptide  
 384 - without the glutamine deletion. The occurrence of putative splicing variants of MEG-12 was  
 385 not confirmed by the second peptide inserted in the EsoCAT construct. More specifically, we  
 386 detected and quantified ENYEQQLQQPK (Smp\_152630.1; both internal standard and  
 387 endogenous analyte present) but not the FHIVFFCGENYEQQLQQPK (Smp\_152630.2; only  
 388 internal standard present), suggesting that the putative splicing variant Smp\_152630.2 lies  
 389 below the instrumental limit of detection (Figure 4).

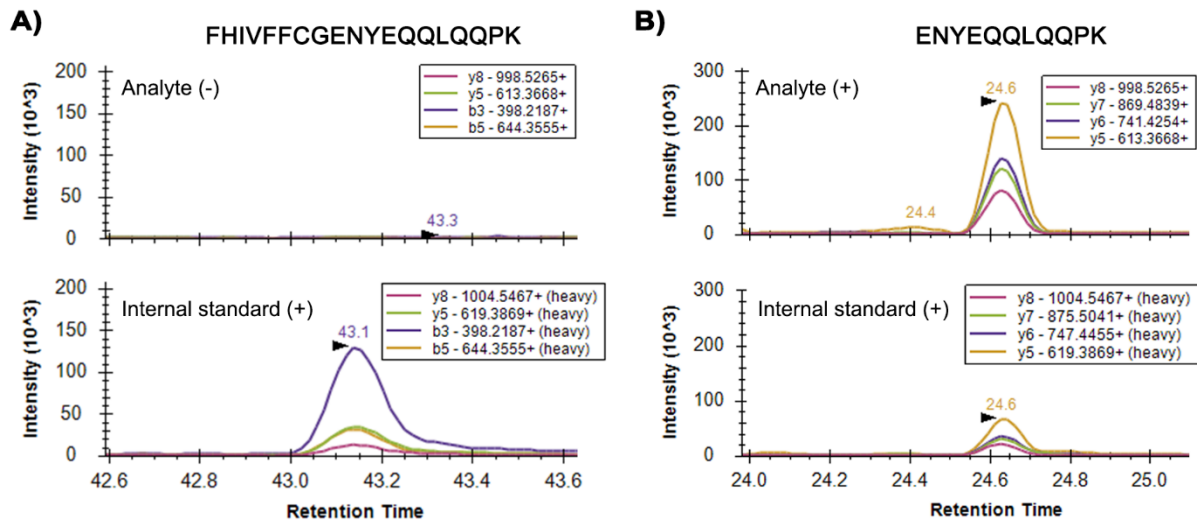


**Figure 4. Proteotypic peptides monitored for MEG-12 quantification.** (A) Extracted ion chromatogram of transitions monitored for FHIVFFCGENYEQLQQPK peptide indicated that the Smp\_152630.2 isoform is below the limit of detection. (B) Conversely, at the same spiking levels of ENYEQLQQPK internal standard the endogenous analyte derived from Smp\_152630.1 isoform is detected.

391 *GO analyses suggest distinctive molecular functions in the worm esophagus*

392 Next, we performed an ESO vs BE comparative analysis using label-free relative

393 quantification. A high similarity between the preparations was observed in the Orbitrap

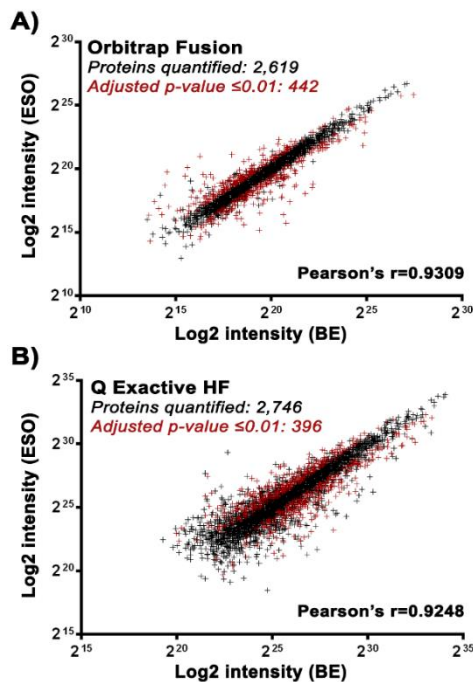


**Figure 5. Shotgun quantitative analysis of ESO and BE samples.** Compositional differences unveiled by label free relative quantification of the data acquired using Orbitrap Fusion (A) and Q Exactive HF (B) indicating, respectively, 442 and 396 differentially abundant proteins (adjusted  $p$ -value  $\leq 0.01$ ,  $\geq 1.5$ -fold difference,  $\geq 2$  unique peptides). Pearson's correlation indicates high similarity between the two preparations ( $R^2 > 0.92$ ).

394 Fusion and Q Exactive HF analysis (Pearson'  $r > 0.9$ ; Figures 5A-B). Nevertheless, a total of  
 395 669 proteins were found differentially abundant in the two platforms together (adjusted p-  
 396 values  $\leq 0.01$ , fold difference  $\geq 1.5$ ,  $\geq 2$  unique peptides; Supplementary Table S1A-B).

397 Functional analysis using STRING database indicated the enrichment of a cluster of  
 398 esophageal proteins involved in glycerophospholipid and sphingolipid metabolism, and  
 399 lysosomal lecithin:cholesterol acyltransferases among the differentially abundant proteins  
 400 (Figure 6; right). On other hand, a remarkable enrichment of proteases in the BE was  
 401 indicated by the overrepresentation of cysteine/papain-like peptidases metalloproteases and  
 402 C1A peptidases (Figure 6; left). The lysosomal pathway and a cluster of proteases/C1A  
 403 peptidases displayed a heterogenous composition with molecules differentially abundant in  
 404 BE and ESO (Figure 6, hashed markers) indicating site-specific activities.

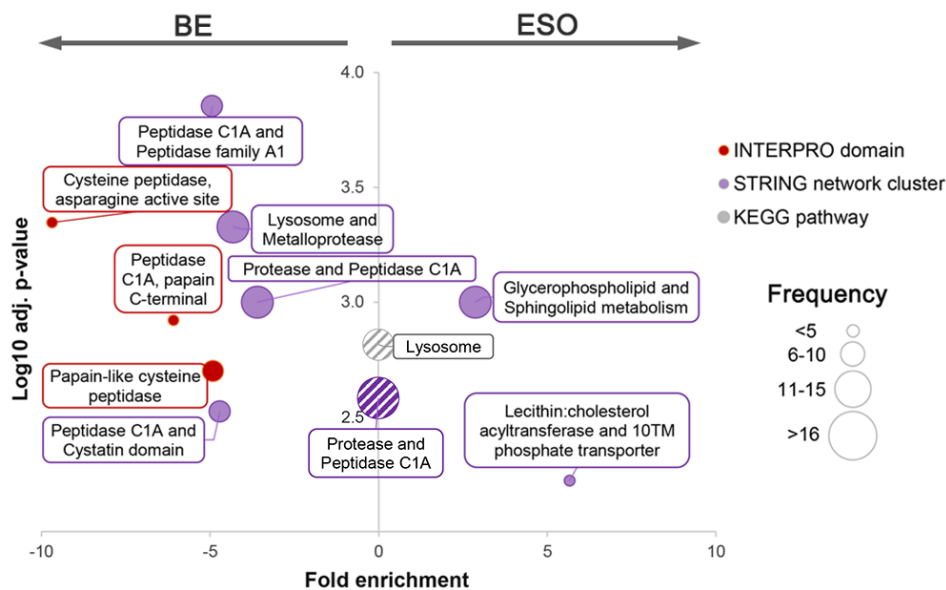


**Figure 6. STRING functional analysis of differentially abundant proteins.** INTERPRO domains associated with proteolytic activity are significantly overrepresented among proteins enriched in the BE (red circles, left). Two clusters of proteins associated with the glycerophospholipid/sphingolipid and lecithin:cholesterol metabolism were detected in the ESO component (purple; right). Constituents of lysosome pathway and a set of proteases/peptidases C1A were enriched in both samples suggesting site-specific activities (hashed circles; centre).

405

406 Next, a GO enrichment analysis was performed by direct comparison of the 359 proteins  
 407 enriched in the male worm's ESO versus the 330 more abundant in the BE. Twenty-three  
 408 over-represented biological processes (FDR  $\leq$  0.05) could be abridged to seven GO terms,  
 409 representing protein biosynthesis and glycosylation, vesicle-mediated transport - including  
 410 Golgi vesicles, oxidation-reduction processes and drug metabolism. Molecular functions and  
 411 cellular components supported the presence of hexosyltransferases, membrane complexes,  
 412 including those in endoplasmic reticulum/Golgi and mitochondrion, as well the  
 413 oxidoreductase complex (Figure 7).

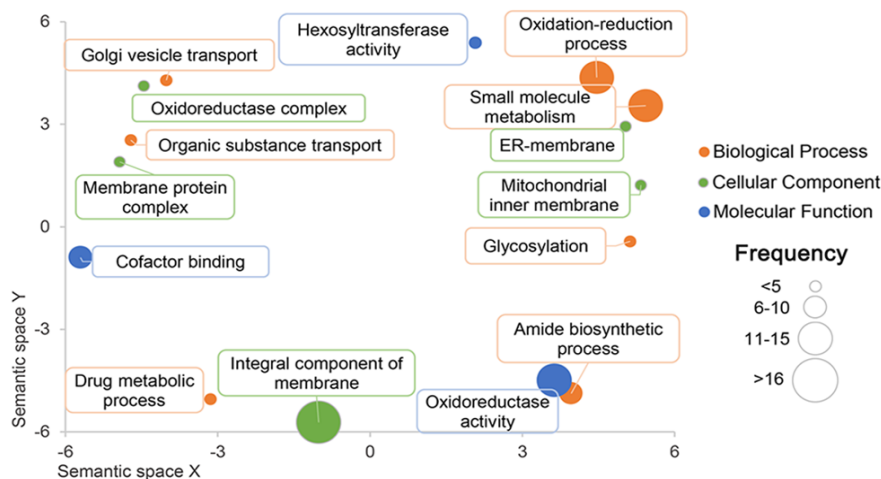


**Figure 7. GO terms over-represented in the ESO compared to BE.** Direct comparison of proteins differentially abundant in the ESO vs BE revealed that GO terms associated with bioenergetics (oxidative phosphorylation), biosynthetic processes (protein biosynthesis and glycosylation) and vesicle-mediated transport are over-represented in the esophagus (FDR $\leq$ 0.05).

414 A closer look at the total of 25 quantified glycosyl transferases showed a greater abundance  
 415 in the esophageal region, by a median factor of 1.8-fold (Figure 8; Supplementary Table  
 416 S1C). Notably, 16 out of 18 differentially abundant glycosyl transferases were enriched in the  
 417 ESO sample. Seven of these are dolichol lipid-linked endoplasmic reticulum transferases.  
 418 Five enzymes with transferase activities spanning galactosyl (Smp\_151220), GalNAc  
 419 (Smp\_057620, Smp\_005500) and mannosyl (Smp\_042790, Smp\_177080, Smp\_102430)  
 420 glycans were also significantly enriched, as were two endoplasmic reticulum glucosidases  
 421 (alpha-mannosidase, Smp\_143430; mannosyl oligosaccharide glucosidase, Smp\_024580).

422 Together, these findings indicate a distinct machinery for production of specialized glycans in  
 423 the esophageal glands.

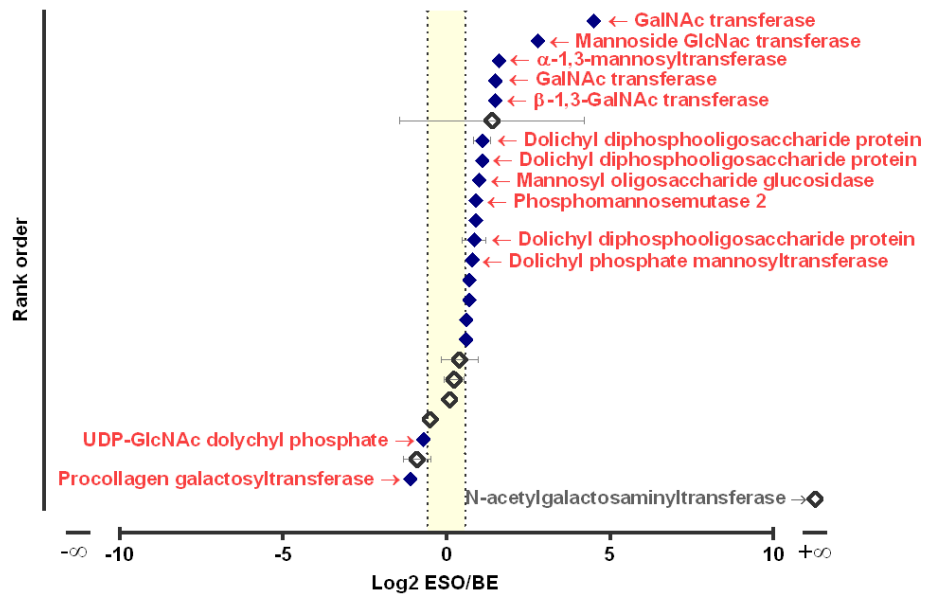


**Figure 8. Differential abundance of glycosyl transferases in the ESO and BE samples.** Diagram showing an enrichment of proteins related to glycosylation processes in the schistosome esophagus (right side). The shaded area indicates the equivalence range (<1.5-fold difference). Proteins are rank ordered according to their average Log2 fold ESO/BE. Differential expression supported by statistical analysis (adjusted p-value  $\leq 0.01$ ) are indicated by solid symbols.

424 STRING analysis of proteins differentially abundant in the ESO revealed a network  
 425 connecting protein biosynthesis, glycosylation and secretory pathways (Figure 9A). Proteins  
 426 involved in a variety of vesicle-trafficking processes featured prominently in the parasite  
 427 esophagus. Those included a tetraspanin CD63 receptor (Smp\_041460; 4.6x-fold difference),  
 428 a non-tegment annexin (Smp\_155580; 37x-fold), charged multivesicular body protein  
 429 (Smp\_079000; 1.5x-fold) and proteins involved in sphingolipid biosynthesis (*e.g.* longevity

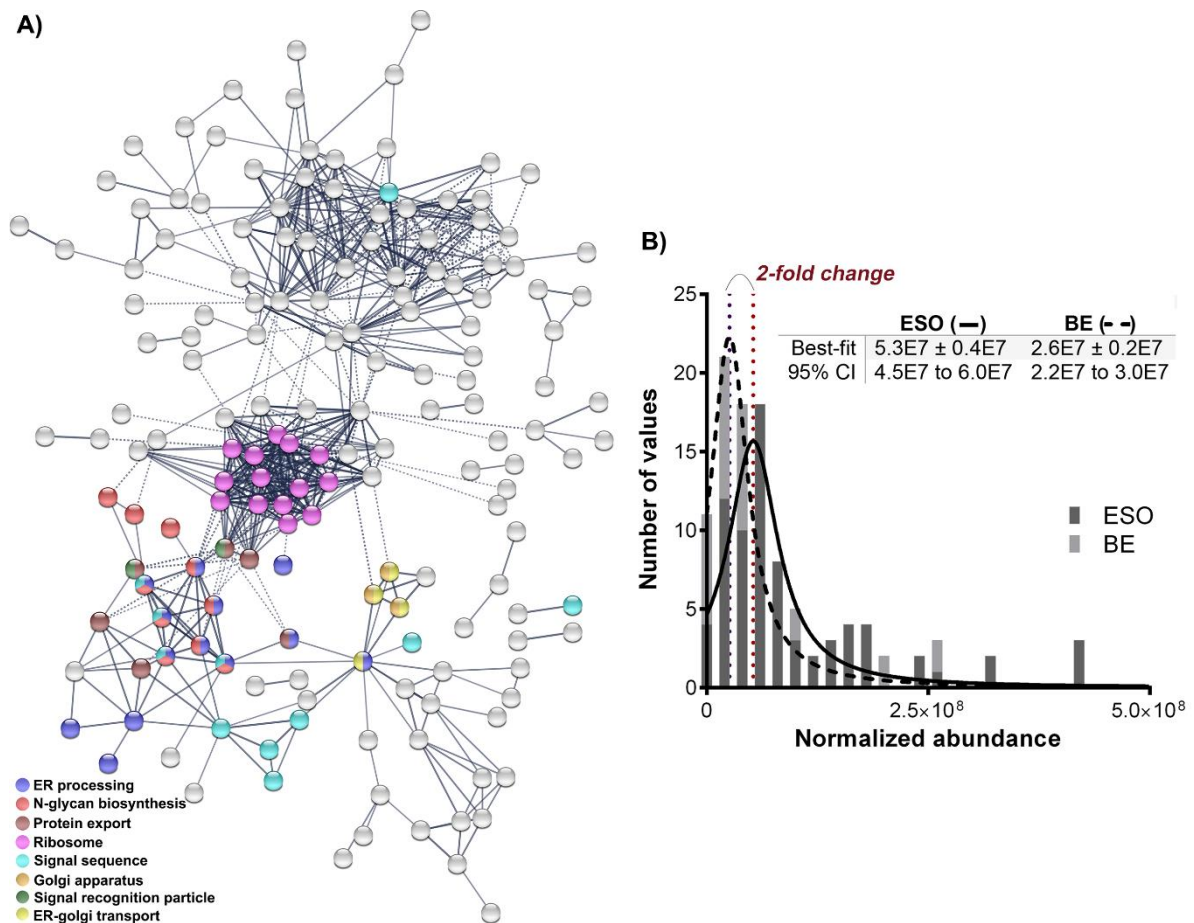


**Figure 9. Network featuring protein biosynthesis, glycosylation and secretion in the schistosome esophagus. (A)** Diagram highlighting the clustering of protein biosynthesis, glycosylation and secretory pathways (coloured circles) among proteins differentially abundant in the ESO. Blank circles are mostly related to bioenergetics and small molecules metabolism. **(B)** Normalised distribution shows an average 2-fold increase on the abundance of proteins associated to vesicle transport and protein secretion. Best-fit values and 95% confidence interval (CI) were calculated using Lorentzian function.

430 assurance gene 1, Smp\_147460, 2.4x-fold; ceramidase, Smp\_122050, 26x-fold; fatty acid  
 431 desaturase 2, Smp\_132740, 8.7x-fold; ormdl protein, Smp\_210370, 1.6x-fold). The  
 432 enrichment of signal recognition particles (*e.g.* SRP-14, 19, 68, 72; average 1.7x-fold  
 433 difference) and signal peptidases (Smp\_031730, Smp\_024390.2 and Smp\_024390.3; average  
 434 1.7x-fold) reinforced that the classical secretory pathway is operational in the esophagus. In  
 435 addition, a number of differentially abundant proteins related to SEC-translocation channels  
 436 (*e.g.* SECs23, 63, 24a, 16a; average 2.1x-fold difference), Coatomer subunits for COPII- and  
 437 COPI-vesicle coat (Smp\_015090, Smp\_031860, Smp\_245450 and Smp\_124430; average  
 438 1.8x-fold difference), translocon-associated proteins (Smp\_075870.1, Smp\_071600,

439 Smp\_074700; average 2.1x-fold difference) and ARF GTPases (Smp\_086900, Smp\_179610;  
440 average 1.8x-fold difference) provides evidence for formation of endoplasmic  
441 reticulum/Golgi secretory vesicles. Altogether, the abundance of all those proteins was  
442 skewed by a factor of 2-fold towards the parasite esophagus (Figure 9B). Of note, similarities  
443 between the esophageal gland and tegument secretion processes led us to inspected our data  
444 for 36 proposed tegument signatures<sup>7</sup>. Their average ESO/BE fold difference was 0.95  
445 indicating an even distribution over the worm surface thus reinforcing that the enrichment we  
446 observed in the ESO preparation is a true reflection of differences in protein composition.

447

448 *Gastrodermal secretions are also pinpointed by the comparative analysis*

449 The results of our ESO vs BE label-free quantification provided the expression pattern of  
450 proteins related to digestive processes over the extent of the esophagus and lower  
451 gastrodermis. Classical gut-associated proteins previously identified in the worm's vomitus<sup>21</sup>  
452 were confirmed as highly enriched in the BE sample (Figure 10; Supplementary Table S1D),  
453 these included cathepsin B1 (Sm31 - Smp\_103610; Smp\_067060), cathepsin S  
454 (Smp\_139240), asparaginyl endopeptidase (Sm32 - Smp\_075800), lysosome-associated  
455 membrane glycoprotein (Smp\_162770) and saposin B (Smp\_014570).

456 On the other hand, we unexpectedly observed that a set of proteins thus far attributed to the  
457 gastrodermis on the basis of vomitus analysis were equally detected in the ESO and BE  
458 samples. For instance, Acyl-CoA thioesterase,  $\beta$ -D-xylosidase, DJ-1/PARK7-like protease,  
459 Nieman Pick C2 (NPC2), vesicle associated membrane protein, lysosomal Pro X  
460 carboxypeptidases (Smp\_002600 and Smp\_071610) and two saposins (Smp\_130100 and  
461 Smp\_016490) did not show statistical differences in relative quantification between the ESO  
462 and BE samples. Furthermore, some vomitus proteins were differentially expressed in the BE  
463 sample but with only a modest enrichment ( $\leq$  2-fold) compared to the ESO; these included



464 ferritin, apoferritin,  $\alpha$ 2-macroglobulin, cathepsins C/D, ester hydrolase, serpin and a saposin  
 465 (Smp\_194910). It is noteworthy to mention that inaccurate dissection could lead to  
 466 contamination of ESO fragments with highly abundant gastrodermis components impairing  
 467 the identification of sample-specific proteins. However, we did not observe any bias  
 468 suggesting that the MS-signal intensity was directly linked to the presence or absence of  
 469 differential expression between ESO and BE (Supplementary Material S5).

470 In addition to the gut-secreted proteins described by Hall *et al.* (2011), we detected other  
 471 molecules potentially related to gastrodermal functions, such as a serine carboxypeptidase  
 472 (Smp\_172590) 22x-fold more abundant in the BE sample. An additional saposin B  
 473 (Smp\_105420; ~5x-fold difference) was also detected significantly enriched in the BE  
 474 supported by only one unique peptide (Supplementary Material S5). Furthermore, the  
 475 expression pattern of cathepsins F/L (Smp\_034410, Smp\_139160 and Smp\_210500), also

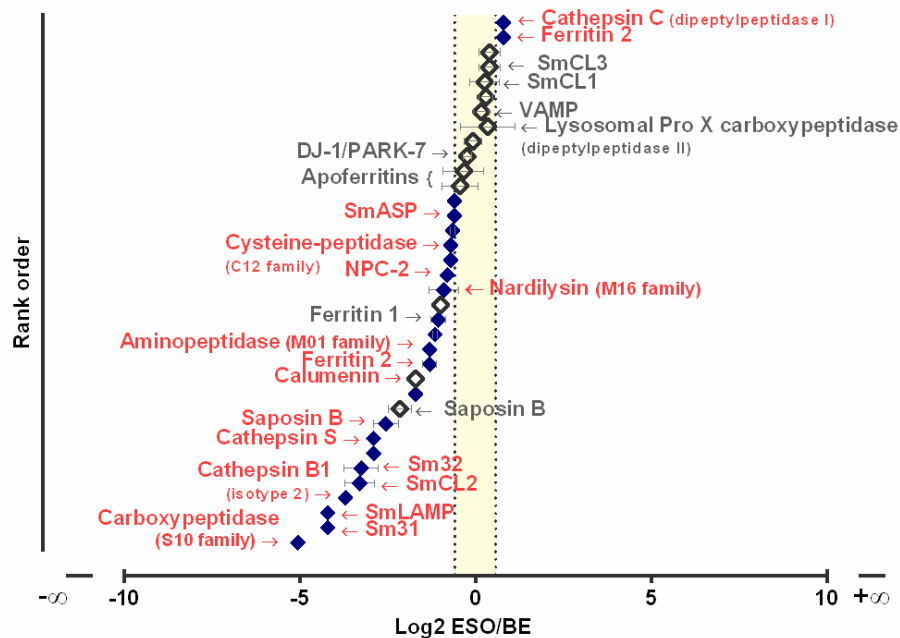


**Figure 10. Differential abundance of putative gut secretions in the ESO and BE samples.** Diagram showing a biased expression (median difference of 1.7x-fold) of gastrodermal markers towards the schistosome back end (left side). Intriguingly, a group of proteins so far attributed to the gastrodermis exhibited an even distribution between the ESO and BE samples (shaded area). Proteins are rank ordered according to their average Log2 fold ESO/BE. Differential expression supported by statistical analysis (adjusted p-value  $\leq 0.01$ ) are indicated by solid symbols.



476 known as SmCL1, SmCL2, SmCL3, revealed that only the second confidently exhibits higher  
477 abundance in the BE sample.

478

## 479 **Discussion**

480 In this work we used quantitative proteomics to assess the composition of the *S. mansoni*  
481 alimentary tract. This investigation allowed us to designate proteins functionally associated  
482 with the anterior and lower regions of the parasite's alimentary tract, namely the esophagus  
483 and gastrodermis, represented by the ESO and BE preparations, respectively. The  
484 combination of a microdissection procedure and relative quantification of these preparations  
485 has permitted the correct assignment of signature proteins to their specific sites of expression.  
486 Particularly, proteins encoded by microexon genes known to be expressed in the anterior and  
487 posterior esophageal glands were detected by proteomics for the first time, expanding our  
488 knowledge of these tissues, thus far limited to transcriptomic analysis<sup>7,8</sup>. This enabled us to  
489 acquire further information on gland constituents by absolute quantification, using QconCAT  
490 methodology. Lastly, ESO vs BE comparisons also provided an informative update of the  
491 repertoire of *S. mansoni* gastrodermal markers.

492 The efficiency of our dissection method for enrichment was firstly confirmed by the ability to  
493 detected specific esophageal MEG proteins (*e.g.* MEG-4.1) and VAL-7 in the ESO sample,  
494 since evidences gathered from independent molecular analysis such as whole-mount *in situ*  
495 hybridisation<sup>28,29</sup>, confocal microscopy and RNA-seq<sup>7</sup> verified their specific expression and  
496 location in the esophageal gland tissues. The successful detection of the putative esophageal  
497 gland secretions can be attributed to substantial enrichment achieved through dissection,  
498 followed by sensitive high-resolution mass spectrometry. Our previous attempts using 2D-  
499 PAGE of the whole male worm heads followed by mass spectrometry, failed to detect a  
500 single genuine gland secretion<sup>9</sup>. Instead, house-keeping proteins and those massively

501 abundant in the major schistosome tissues (*i.e.* sucker and body wall muscles, and  
502 parenchyma) dominated the preparation. Similarly, shotgun proteomics of soluble parasite  
503 components using modern LC-MS instrumentation was also inefficient for the detection of  
504 such low abundance antigens <sup>11</sup>.

505 Although the exact functions of MEG proteins have yet to be demonstrated, most display  
506 peculiar structural elements and low homology outside the *Schistosoma* genus, suggesting  
507 they may possess unique roles in worm physiology. The unusual structure of these genes,  
508 mainly composed of short (<36bp) and symmetric exons (multiple of three bases), allows the  
509 generation of several variants by alternative splicing events without disrupting the reading  
510 frame <sup>30</sup>, thus preserving the main protein backbone. In fact, the expression of multiple MEG  
511 isoforms was confirmed in our data. It has been hypothesised that these variation events  
512 could be linked to evasion mechanisms deployed under a selective pressure created by the  
513 host immune system <sup>12</sup>. More specifically, the amino acid substitution observed for MEGs 4.1  
514 and 4.2 corroborate the previously reported high synonymous and nonsynonymous  
515 substitution rates (dN/dS) in schistosome microexon genes <sup>31</sup>. It is noteworthy that high  
516 dN/dS rates have been reported for antigens constantly exposed at host-parasite interfaces  
517 (*e.g.* gut secretions and tegument exposed proteins), including the vaccine candidates Sm29  
518 and Tetraspanin-2 (Sm-TSP2), and VAL proteins <sup>31</sup>. This could in fact anticipate that  
519 esophageal MEGs are targeted by the host immune response and might constitute a set of  
520 new vaccine candidates. However, we must bear in mind that in those cases, sequence  
521 variation has to be contemplated during vaccine design since the accumulation of antigenic  
522 diversity might impair the outcome of the protective immunization <sup>32</sup>.

523 Faced with a complex repertoire of putative gland secreted proteins, it may be beneficial to  
524 design new vaccines against the most abundant candidate molecules. Since the MEG proteins  
525 display short sequences, lack conserved protein domains and are likely to possess

526 intrinsically disordered structures<sup>33</sup>, it is unlikely these molecules exhibit any catalytic  
527 activity. This led us to hypothesise that their abundance in the parasite esophagus may reflect  
528 the rate at which these proteins are consumed by interaction with incoming blood. Absolute  
529 quantification revealed MEG-12 as the most abundant target protein per cell, among the nine  
530 putative gland secretions evaluated in the QconCAT assay. Specific expression of MEG-12 in  
531 the anterior esophageal gland of male and female adult worms was confirmed by whole  
532 mount *in-situ* hybridization<sup>7</sup>, and together these data may suggest it could play an important  
533 role in the first contact with incoming blood. So far, MEG-12 has been proposed to function  
534 by interacting with erythrocytes and promoting hemolysis through a predicted amphipatic  
535 helix<sup>7</sup>. VAL-7 and MEG 4 family proteins, all secreted by the posterior gland, also exhibited  
536 a high number of copies per cell and is reinforced by high expression of the cognate  
537 transcripts, as already revealed by microarray and quantitative RNAseq<sup>7,29,34</sup>.

538 The esophageal glands and the syncytial gastrodermis are the major secretory structures in  
539 the upper and lower alimentary tract, respectively<sup>35</sup>. Our results showed that GO terms  
540 related to secretion via vesicle transport are significantly overrepresented among proteins  
541 differentially expressed in the ESO proteome when compared with the BE. The remarkable  
542 expression of molecules tightly related to vesicle-trafficking such as a tetraspanin CD63  
543 receptor and a non-tegument annexin (Smp\_155580), as well as proteins related to  
544 sphingolipid biosynthesis, might constitute a route for a therapeutic intervention. In  
545 particular, annexins have been proposed as potential drug and vaccine targets because of their  
546 important role in secretory processes and exposure to the host immune system<sup>36</sup>. Notably,  
547 disrupting vesicle release in the esophageal lumen has been implicated in the self-cure  
548 response of the Rhesus macaque<sup>6</sup>.

549 The highlighted activity of secretory pathways is probably linked to the repertoire of  
550 glycosyltransferases differentially abundant in the schistosome esophagus. The enrichment of

551 proteins linked to N- and O-glycosylation in the ESO sample matches the requirement of a  
552 specialised machinery for decorating gland products with specific glycan moieties. Notably,  
553 the enrichment of beta-1,3-galactosyltransferase and GalNAc transferases in the esophageal  
554 region indicates a favourable environment for production of glycoproteins modified with  
555 galactosyl ( $\beta$ -1,3) N-acetylgalactosamine, which may explain the strong reactivity of the  
556 lectin PNA (peanut agglutinin) towards the esophageal glands <sup>37</sup>. In previous experiments we  
557 demonstrated MEG-4.1 as one of the PNA-reactive antigens, based on bidimensional western  
558 blotting <sup>9</sup>. Remarkably, MEG-4.1 reactivity was shown split into two spots, indicating either  
559 the presence of glycoforms or alternatively spliced sequences. We acknowledge that several  
560 O-glycosylation sites predicted for MEG-4.1 are located within a tandemly repeated  
561 sequence. Detection of non-decorated peptides derived from this region suggests that  
562 glycosylation can be differential. However, the extent of the glycosylation over the repetitive  
563 sequence cannot be inferred from bottom-up proteomics. Nevertheless, unceasing production  
564 of fully glycosylated forms would require constant availability of glycan precursors. This  
565 condition might not be fulfilled since esophageal MEG proteins are the most rapidly  
566 synthesised, during *in vitro* turnover experiments (manuscript in preparation). In future  
567 investigations it would be beneficial to characterise the extent and type of glycans linked to  
568 the protein antigens of interest.

569 Finally, we interrogated our data for proteins known to be present in the worm vomitus <sup>21</sup>.  
570 Although gut secretions dominate these preparations, additional components originated from  
571 the esophagus, including MEG proteins (manuscript in preparation) and molecules released  
572 from the membranocalyx were among the secreted molecules. In this context, our quantitative  
573 ESO vs BE analysis provided additional information regarding the preferential site of  
574 expression of many proteins so far attributed to the gastrodermis. Although regurgitation of  
575 gut content and imprecise dissection might contribute unwanted contamination by

576 gastrodermal secretions in the esophageal lumen we didn't observe any bias suggesting that  
577 our ESO preparation had significant contamination with abundant gut secretions. Classical  
578 gut-associated antigens such as Sm31 and Sm32, were highly expressed in the BE, enzymes  
579 and transporters such as Acyl-CoA thioesterase, beta-D-xylosidase, NPC2, and some  
580 saposins were shown to be equally abundant in both ESO and BE fragments. This might  
581 suggest that some hydrolases thought to be exclusive to the gut compartment do in fact  
582 function in unrelated worm tissues not resolved by the ESO *vs* BE approach. For instance,  
583 this might include lipid and cholesterol binding and transport – by saposins and NPC2 – and  
584 iron binding by ferritin, by lysosomes in other tissue locations.

585 Moreover, we highlight that the ESO *vs* BE comparison provided new information on a group  
586 of cathepsins. SmCL1, CL2 and CL3 have been reported as specific gastrodermal  
587 constituents<sup>38,39</sup>. However, only SmCL2 was enriched in the BE sample. This might indicate  
588 that both SmCL1 and SmCL3 exhibit a more promiscuous biological role in other tissues,  
589 besides blood digestion in the parasite intestine. Differences in the pH optima of these  
590 enzymes should be considered. Whilst SmCL2 activity is restricted to acidic environments,  
591 such as that found in the parasite gut lumen, SmCL1 exhibits a broad pH profile (80% at pH  
592 5-7.2, optimum pH 6.5)<sup>40</sup>, similar to SmCL3<sup>39</sup>. Therefore, our data suggest SmCL2 as the  
593 only member among SmCL peptidases, that is solely active in the schistosome gut.

594

## 595 **Conclusion**

596 The schistosome feeding process is multistep and takes place within three chambers, clearly  
597 demarcated along the alimentary tract, namely the anterior and posterior esophageal lumen  
598 and the gut proper<sup>35</sup>. Unlike the gut, proteomic analysis of esophageal secretions produced  
599 by the esophageal glands has not previously been attempted since isolation of this  
600 microproteome is challenging. In this study we developed a dissection technique enabling the

601 generation of esophageal fragments for detailed characterisation of the *S. mansoni* esophagus.  
602 Our results revealed a complex protein composition in the esophageal region with evidence  
603 of antigenic variation of MEG-encoded proteins that might have serious implications in  
604 immune evasion. Nevertheless, the remarkable abundance of esophageal MEG proteins  
605 suggests a high demand for those constituents in the incessant blood processing cascade. In  
606 addition, dissection of the esophagus versus the back end provided an overview of differential  
607 biological processes enriched in the two body fragments, as well as updating the repertoire of  
608 proteins involved in the later steps of blood digestion and nutrient acquisition. Together, our  
609 data provide the basis for a better-oriented selection of alimentary tract candidates for vaccine  
610 development.

611

#### 612 **Competing interests**

613 The authors declare that they have no competing interests.

614

#### 615 **SUPPORTING INFORMATION**

616 The following supporting information is available free of charge at ACS website

617 <http://pubs.acs.org>

618 Supplementary Material S1\_ Expanded methodology of shotgun proteomic analyses

619 Supplementary Material S2\_ EsoCAT construct, heterologous expression and monitored

620 transitions

621 Supplementary Material S3\_ Identification and relative quantification of MEG proteins

622 Supplementary Material S4\_ Descriptive statistics of QconCAT assay and protein copy per

623 cell estimation

624 Supplementary Material S5\_ Abundance of gastrodermis markers and statistical differences

625 Supplementary Table S1\_ Label-free quantification and tissue signatures.xlsx

626 Supplementary Table S2\_ QconCAT absolute quantification.xlsx

627

628 **Data availability statement**

629 The shotgun mass spectrometry proteomics data have been deposited to the  
630 ProteomeXchange Consortium via the PRIDE partner repository <sup>41</sup> with the dataset identifiers  
631 PXD014872 and 10.6019/PXD014872. The SRM analyses are available on Panorama Public  
632 at the following link <https://panoramaweb.org/PCTZUp.url> and ProteomeXchange identifier  
633 PXD014899. Skyline exported data for all quantified peptides are available in Supplementary  
634 Table S2.

635

636 **Author's contribution**

637 LXN designed and carried out the experiments, analysed and interpreted data, and wrote the  
638 manuscript. RAW and WCB designed experiments, analysed data and wrote the manuscript.  
639 PB, VMH, SWH, RJB and CEE assisted experiment design, offered technical expertise and  
640 contributed to interpretation of data. RM offered technical expertise and contributed with data  
641 interpretation. All authors reviewed the manuscript.

642

643 **Acknowledgments**

644 The authors acknowledge Fundação Oswaldo Cruz (Centro de Pesquisas René Rachou, Belo  
645 Horizonte, Brazil) for providing cercariae for animal infection.

646

647 **Funding sources**

648 This study was financed in part by the Coordenação de Aperfeiçoamento de Pessoal de Nível  
649 Superior - Brasil (CAPES) - Finance Code 001 - by providing a PhD scholarship to LXN.  
650 WCB received funding from Fundação de Amparo à Pesquisa do Estado de Minas Gerais  
651 (FAPEMIG) - grant numbers APQ-00829-15 and APQ-03367-16. CEE, RJB and PB received

652 funding from Biotechnology and Biological Sciences Research Council (BBSRC) grant

653 number BB/M012557/1.

654



655 REFERENCES

- 656 (1) World Health Organization. Schistosomiasis [http://www.who.int/news-room/fact-](http://www.who.int/news-room/fact-sheets/detail/schistosomiasis)  
657 [sheets/detail/schistosomiasis](http://www.who.int/news-room/fact-sheets/detail/schistosomiasis) (accessed Sep 26, 2018).
- 658 (2) Kittur, N.; Castleman, J. D.; Campbell, C. H.; King, C. H.; Colley, D. G. Comparison  
659 of *Schistosoma mansoni* Prevalence and Intensity of Infection, as Determined by the  
660 Circulating Cathodic Antigen Urine Assay or by the Kato-Katz Fecal Assay: A  
661 Systematic Review. *Am J Trop Med Hyg* **2016**, *94* (3), 605–610.
- 662 (3) Secor, W. E.; Montgomery, S. P. Something Old, Something New: Is Praziquantel  
663 Enough for Schistosomiasis Control? *Future Med Chem* **2015**, pp 681–684.
- 664 (4) Molehin, A. J.; Rojo, J. U.; Siddiqui, S. Z.; Gray, S. A.; Carter, D.; Siddiqui, A. A.  
665 Development of a Schistosomiasis Vaccine. *Expert Rev Vaccines* **2016**, *15* (5), 619–  
666 627.
- 667 (5) Wilson, R. A.; Langermans, J. A.; van Dam, G. J.; Vervenne, R. A.; Hall, S. L.;  
668 Borges, W. C.; Dillon, G. P.; Thomas, A. W.; Coulson, P. S. Elimination of  
669 *Schistosoma mansoni* Adult Worms by Rhesus Macaques: Basis for a Therapeutic  
670 Vaccine? *PLoS Negl Trop Dis* **2008**, *2* (9), e290.
- 671 (6) Li, X. H.; Xu, Y. X.; Vance, G.; Wang, Y.; Lv, L. B.; van Dam, G. J.; Cao, J. P.;  
672 Wilson, R. A. Evidence That Rhesus Macaques Self-Cure from a *Schistosoma*  
673 *japonicum* Infection by Disrupting Worm Esophageal Function: A New Route to an  
674 Effective Vaccine? *PLoS Negl Trop Dis* **2015**, *9* (7), e0003925.
- 675 (7) Wilson, R. A.; Li, X. H.; MacDonald, S.; Neves, L. X.; Vitoriano-Souza, J.; Leite, L.  
676 C. C.; Farias, L. P.; James, S.; Ashton, P. D.; DeMarco, R.; et al. The Schistosome  
677 Esophagus Is a ‘Hotspot’ for Microexon and Lysosomal Hydrolase Gene Expression:  
678 Implications for Blood Processing. *PLoS Negl Trop Dis* **2015**, *9* (12), e0004272.
- 679 (8) Li, X. H.; DeMarco, R.; Neves, L. X.; James, S. R.; Newling, K.; Ashton, P. D.; Cao,

- 680 J. P.; Wilson, R. A.; Castro-Borges, W. Microexon Gene Transcriptional Profiles and  
681 Evolution Provide Insights into Blood Processing by the *Schistosoma japonicum*  
682 Esophagus. *PLoS Negl Trop Dis* **2018**, *12* (2), e0006235.
- 683 (9) Li, X. H.; de Castro-Borges, W.; Parker-Manuel, S.; Vance, G. M.; DeMarco, R.;  
684 Neves, L. X.; Evans, G. J. O.; Wilson, R. A. The Schistosome Oesophageal Gland:  
685 Initiator of Blood Processing. *PLoS Negl Trop Dis* **2013**, *7* (7), e2337.
- 686 (10) Skelly, P. J.; Da'dara, A. A.; Li, X. H.; Castro-Borges, W.; Wilson, R. A. Schistosome  
687 Feeding and Regurgitation. *PLoS Pathog* **2014**, *10* (8), e1004246.
- 688 (11) Neves, L. X.; Sanson, A. L.; Wilson, R. A.; Castro-Borges, W. What's in SWAP?  
689 Abundance of the Principal Constituents in a Soluble Extract of *Schistosoma mansoni*  
690 Revealed by Shotgun Proteomics. *Parasit Vectors* **2015**, *8* (1), 337.
- 691 (12) DeMarco, R.; Mathieson, W.; Manuel, S. J.; Dillon, G. P.; Curwen, R. S.; Ashton, P.  
692 D.; Ivens, A. C.; Berriman, M.; Verjovski-Almeida, S.; Wilson, R. A. Protein  
693 Variation in Blood-Dwelling Schistosome Worms Generated by Differential Splicing  
694 of Micro-Exon Gene Transcripts. *Genome Res* **2010**, *20* (8), 1112–1121.
- 695 (13) Orcia, D.; Zeraik, A. E.; Lopes, J. L. S.; Macedo, J. N. A.; Santos, C. R. D.; Oliveira,  
696 K. C.; Anderson, L.; Wallace, B. A.; Verjovski-Almeida, S.; Araujo, A. P. U.; et al.  
697 Interaction of an Esophageal MEG Protein from Schistosomes with a Human S100  
698 Protein Involved in Inflammatory Response. *Biochim Biophys Acta* **2017**, *1861* (1 Pt  
699 A), 3490–3497.
- 700 (14) Pratt, J. M.; Simpson, D. M.; Doherty, M. K.; Rivers, J.; Gaskell, S. J.; Beynon, R. J.  
701 Multiplexed Absolute Quantification for Proteomics Using Concatenated Signature  
702 Peptides Encoded by QconCAT Genes. *Nat Protoc* **2006**, *1* (2), 1029–1043.
- 703 (15) Beynon, R. J.; Doherty, M. K.; Pratt, J. M.; Gaskell, S. J. Multiplexed Absolute  
704 Quantification in Proteomics Using Artificial QCAT Proteins of Concatenated

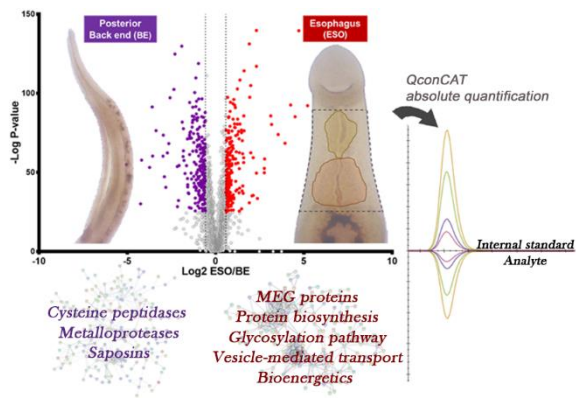
- 705 Signature Peptides. *Nat Methods* **2005**, 2 (8), 587–589.
- 706 (16) Teytelman, L. No More Excuses for Non-Reproducible Methods. *Nature* **2018**, 560  
707 (7719), 411–411.
- 708 (17) Bennett, R. J.; Simpson, D. M.; Holman, S. W.; Ryan, S.; Brownridge, P.; Eyers, C.  
709 E.; Colyer, J.; Beynon, R. J. DOSCATs: Double Standards for Protein Quantification.  
710 *Sci Rep* **2017**, 7, 45570.
- 711 (18) Zhang, J.; Xin, L.; Shan, B.; Chen, W.; Xie, M.; Yuen, D.; Zhang, W.; Zhang, Z.;  
712 Lajoie, G. A.; Ma, B. PEAKS DB: De Novo Sequencing Assisted Database Search for  
713 Sensitive and Accurate Peptide Identification. *Mol Cell Proteomics* **2012**, 11 (4),  
714 M111.010587.
- 715 (19) Götz, S.; García-Gómez, J. M.; Terol, J.; Williams, T. D.; Nagaraj, S. H.; Nueda, M.  
716 J.; Robles, M.; Talón, M.; Dopazo, J.; Conesa, A. High-Throughput Functional  
717 Annotation and Data Mining with the Blast2GO Suite. *Nucleic Acids Res.* **2008**, 36  
718 (10), 3420–3435.
- 719 (20) Szklarczyk, D.; Gable, A. L.; Lyon, D.; Junge, A.; Wyder, S.; Huerta-Cepas, J.;  
720 Simonovic, M.; Doncheva, N. T.; Morris, J. H.; Bork, P.; et al. STRING V11: Protein–  
721 Protein Association Networks with Increased Coverage, Supporting Functional  
722 Discovery in Genome-Wide Experimental Datasets. *Nucleic Acids Res.* **2019**, 47 (D1),  
723 D607–D613.
- 724 (21) Hall, S. L.; Braschi, S.; Truscott, M.; Mathieson, W.; Cesari, I. M.; Wilson, R. A.  
725 Insights into Blood Feeding by Schistosomes from a Proteomic Analysis of Worm  
726 Vomitus. *Mol Biochem Parasitol* **2011**, 179 (1), 18–29.
- 727 (22) Eyers, C. E.; Lawless, C.; Wedge, D. C.; Lau, K. W.; Gaskell, S. J.; Hubbard, S. J.  
728 CONSeQuence: Prediction of Reference Peptides for Absolute Quantitative  
729 Proteomics Using Consensus Machine Learning Approaches. *Mol Cell Proteomics*

- 730           **2011**, *10* (11), M110 003384.
- 731   (23) Cheung, C. S.; Anderson, K. W.; Wang, M.; Turko, I. V. Natural Flanking Sequences  
732           for Peptides Included in a Quantification Concatamer Internal Standard. *Anal Chem*  
733           **2015**, *87* (2), 1097–1102.
- 734   (24) Brownridge, P. J.; Harman, V. M.; Simpson, D. M.; Beynon, R. J. Absolute  
735           Multiplexed Protein Quantification Using QconCAT Technology. In *Quantitative*  
736           *Methods in Proteomics*; Marcus, K., Ed.; Humana Press: Totowa, NJ, **2012**; pp 267–  
737           293.
- 738   (25) MacLean, B.; Tomazela, D. M.; Shulman, N.; Chambers, M.; Finney, G. L.; Frewen,  
739           B.; Kern, R.; Tabb, D. L.; Liebler, D. C.; MacCoss, M. J. Skyline: An Open Source  
740           Document Editor for Creating and Analyzing Targeted Proteomics Experiments.  
741           *Bioinformatics* **2010**, *26* (7), 966–968.
- 742   (26) Reiter, L.; Rinner, O.; Picotti, P.; Huttenhain, R.; Beck, M.; Brusniak, M. Y.;  
743           Hengartner, M. O.; Aebersold, R. mProphet: Automated Data Processing and  
744           Statistical Validation for Large-Scale SRM Experiments. *Nat Methods* **2011**, *8* (5),  
745           430–435.
- 746   (27) Brownridge, P.; Holman, S. W.; Gaskell, S. J.; Grant, C. M.; Harman, V. M.; Hubbard,  
747           S. J.; Lanthaler, K.; Lawless, C.; O’Cualain, R.; Sims, P.; et al. Global Absolute  
748           Quantification of a Proteome: Challenges in the Deployment of a QconCAT Strategy.  
749           *Proteomics* **2011**, *11* (15), 2957–2970.
- 750   (28) Rofatto, H. K.; Parker-Manuel, S. J.; Barbosa, T. C.; Tararam, C. A.; Alan Wilson, R.;  
751           Leite, L. C. C.; Farias, L. P. Tissue Expression Patterns of *Schistosoma mansoni*  
752           Venom Allergen-Like Proteins 6 and 7. *Int J Parasitol* **2012**, *42* (7), 613–620.
- 753   (29) Dillon, G. P.; Illes, J. C.; Isaacs, H. V; Wilson, R. A. Patterns of Gene Expression in  
754           Schistosomes: Localization by Whole Mount in Situ Hybridization. *Parasitology* **2007**,

- 755 134 (Pt 11), 1589–1597.
- 756 (30) Berriman, M.; Haas, B. J.; LoVerde, P. T.; Wilson, R. A.; Dillon, G. P.; Cerqueira, G.  
757 C.; Mashiyama, S. T.; Al-Lazikani, B.; Andrade, L. F.; Ashton, P. D.; et al. The  
758 Genome of the Blood Fluke *Schistosoma mansoni*. *Nature* **2009**, *460* (7253), 352–358.
- 759 (31) Philippsen, G. S.; Wilson, R. A.; DeMarco, R. Accelerated Evolution of Schistosome  
760 Genes Coding for Proteins Located at the Host-Parasite Interface. *Genome Biol Evol*  
761 **2015**, *7* (2), 431–443.
- 762 (32) Xu, X.; Sun, J.; Zhang, J.; Wellems, D.; Qing, X.; McCutchan, T.; Pan, W. Having a  
763 Pair: The Key to Immune Evasion for the Diploid Pathogen *Schistosoma japonicum*.  
764 *Sci Rep* **2012**, *2* (1), 346.
- 765 (33) Lopes, J. L. S.; Orcia, D.; Araujo, A. P. U.; DeMarco, R.; Wallace, B. A. Folding  
766 Factors and Partners for the Intrinsically Disordered Protein Micro-Exon Gene 14  
767 (MEG-14). *Biophys J* **2013**, *104* (11), 2512.
- 768 (34) Parker-Manuel, S. J.; Ivens, A. C.; Dillon, G. P.; Wilson, R. A. Gene Expression  
769 Patterns in Larval *Schistosoma mansoni* Associated with Infection of the Mammalian  
770 Host. *PLoS Negl Trop Dis* **2011**, *5* (8), e1274.
- 771 (35) Li, X. H.; Wilson, R. A. Alimentary Tract of *Schistosoma*. In *Schistosoma: Biology,*  
772 *Pathology and Control*; Jamieson, B. G. M., Ed.; CRC Press, **2016**; Vol. 1, pp 239–  
773 271.
- 774 (36) Hofmann, A.; Osman, A.; Leow, C. Y.; Driguez, P.; McManus, D. P.; Jones, M. K.  
775 Parasite Annexins--New Molecules with Potential for Drug and Vaccine Development.  
776 *Bioessays* **2010**, *32* (11), 967–976.
- 777 (37) Collins, J. J.; King, R. S.; Cogswell, A.; Williams, D. L.; Newmark, P. A. An Atlas for  
778 *Schistosoma mansoni* Organs and Life-Cycle Stages Using Cell Type-Specific  
779 Markers and Confocal Microscopy. *PLoS Negl Trop Dis* **2011**, *5* (3), e1009.

- 780 (38) Bogitsh, B. J.; Dalton, J. P.; Brady, C. P.; Brindley, P. J. Gut-Associated  
781 Immunolocalization of the *Schistosoma mansoni* Cysteine Proteases, SmCL1 and  
782 SmCL2. *J Parasitol* **2001**, *87* (2), 237–241.
- 783 (39) Dvořák, J.; Mashiyama, S. T.; Sajid, M.; Braschi, S.; Delcroix, M.; Schneider, E. L.;  
784 McKerrow, W. H.; Bahgat, M.; Hansell, E.; Babbitt, P. C.; et al. SmCL3, a  
785 Gastrodermal Cysteine Protease of the Human Blood Fluke *Schistosoma mansoni*.  
786 *PLoS Negl Trop Dis* **2009**, *3* (6), e449.
- 787 (40) Brady, C. P.; Brindley, P. J.; Dowd, A. J.; Dalton, J. P. *Schistosoma mansoni*:  
788 Differential Expression of Cathepsins L1 and L2 Suggests Discrete Biological  
789 Functions for Each Enzyme. *Exp Parasitol* **2000**, *94* (2), 75–83.
- 790 (41) Perez-Riverol, Y.; Csordas, A.; Bai, J.; Bernal-Llinares, M.; Hewapathirana, S.;  
791 Kundu, D. J.; Inuganti, A.; Griss, J.; Mayer, G.; Eisenacher, M.; et al. The PRIDE  
792 Database and Related Tools and Resources in 2019: Improving Support for  
793 Quantification Data. *Nucleic Acids Res.* **2019**, *47* (D1), D442–D450.
- 794

795 For TOC Only



796